Applied Catalysis B: Environmental 322 (2023) 122074

Contents lists available at ScienceDirect

Applied Catalysis B: Environmental

journal homepage: www.elsevier.com/locate/apcatb

Effect of framework Al pairing on NO storage properties of Pd-CHA passive NOx adsorbers

Joseph R. Theis [a], Justin Ura [a], Andrew Bean Getsoian [a], Vitaly Y. Prikhodko [b], Calvin R. Thomas [b], Josh A. Pihl [b], Trevor M. Lardinois [c], Rajamani Gounder [c], Xinyi Wei [d], Yaying Ji [e], Robert B. Pace [e], Mark Crocker [e,*]

[a] Applied Sciences, Ford Motor Company, 2101 Village Road, Dearborn, MI 48124, USA
[b] Oak Ridge National Laboratory, 1 Bethel Valley Road, Oak Ridge, TN 37830, USA
[c] Charles D. Davidson School of Chemical Engineering, Purdue University, West Lafayette, IND 47907, USA
[d] BASF Corporation, 25 Middlesex-Essex Turnpike, Iselin, NJ 08830, USA
[e] Center for Applied Energy Research, University of Kentucky, Lexington, KY 40511, USA

ARTICLE INFO

Keywords:
PNA
LTNA
Low temperature NOx adsorber
Chabazite
SSZ-13
Framework Al
Paired Al sites

ABSTRACT

Three Pd/H-CHA samples were prepared containing 53.0 %, 10.8 % and 6.5 % paired Al sites at near fixed Si/Al ratio and similar Pd loading. According to H_2 temperature-programmed reduction, Pd was present almost exclusively as isolated cations in the two samples containing the higher concentrations of paired Al sites, whereas in the other sample PdO was also present. Simulated lean cold start tests on the fresh samples conducted in a microflow reactor showed that the sample containing PdO stored the lowest amount of NOx. When tested with CO/H_2, the sample containing 53.0 % paired Al sites showed significantly better storage capacity than the other samples and deactivated less rapidly upon sequential tests. Experiments using lean gasoline engine exhaust revealed similar trends. This study showed that a high concentration of paired Al sites in Pd/H-CHA is beneficial for NOx storage capacity, thermal durability, and minimizing deactivation in the presence of CO/H_2.

1. Introduction

The low exhaust temperatures that result from improvements to engine efficiency represent a challenge to the control of pollutant emissions. Standard aftertreatment technologies such as three-way catalysts (TWCs) and selective catalytic reduction (SCR) catalysts fail to function efficiently at low temperatures, from which it follows that high efficiency internal combustion engines require new or improved aftertreatment technologies that specifically address this issue. Passive NO_x adsorbers (PNAs), also known as low temperature NOx adsorbers (LTNAs), represent a possible strategy to mitigate these emissions, with palladium-loaded zeolites being of particular interest [1–3]. The intended function of these materials is to adsorb NO_x and hydrocarbons at low temperatures (~25–200 °C) and then to desorb them once the downstream catalytic converter has reached operational temperature (>200 °C) [4]. Several characteristics are required for a material to serve as a PNA, including adsorption of large quantities of NO_x (and particularly NO) at near ambient temperature and complete desorption of the stored NO_x species at temperatures that are within the range of exhaust temperatures on the vehicle during normal customer usage (typically no more than 300–350 °C for diesel vehicles). These materials must also resist the detrimental effects of all typical exhaust components (e.g., H_2O, CO_2, CO, H_2, HC, SO_2, etc.) over a wide range of temperature for the useful life of the vehicle.

Recent studies have shown that under working conditions, the NO adsorption sites in Pd zeolites correspond to isolated Pd cations, including Pd^{2+} and Pd^{+} [5–10]. Depending on a number of factors related to material structure and preparation, including the zeolite framework topology, synthesis and treatment conditions, and the framework Al content and extent of Al pairing in the framework, other Pd species may be present in as-prepared Pd zeolite samples in the form of metallic Pd and PdO (in nanoparticulate or bulk form) [11,12]. NO can also adsorb at acid sites (H^{+}) in the zeolite framework that are generated upon isomorphous substitution of framework Si with Al, although such adsorption is suppressed in the presence of water vapor [1,3,13]. The presence of Pd^{2+} ions in these materials has been

* Corresponding author.
E-mail address: mark.crocker@uky.edu (M. Crocker).

https://doi.org/10.1016/j.apcatb.2022.122074
Received 1 July 2022; Received in revised form 10 October 2022; Accepted 11 October 2022
Available online 13 October 2022

substantiated by a variety of methods, including X-ray photoelectron spectroscopy, diffuse reflectance UV–vis spectroscopy, X-ray absorption spectroscopy, and H_2 temperature programmed-reduction (TPR) [11,14]. Spectroscopic evidence for the presence of Pd^+ exists in the form of IR spectra collected using CO [15,16] and NO [17–19] as probe molecules, while electron paramagnetic resonance measurements have indicated the presence of Pd^+ in Pd zeolites exposed to reducing conditions [20,21]. Indeed, the formation of Pd^+ from Pd^{2+} has been reported to occur upon NO adsorption in Pd/H-ZSM-5 [18,19], with the Pd^{2+} species undergoing reduction being assigned as either isolated Pd^{2+} ions or Pd^{2+} hydroxyl complexes (i.e., $[Pd(OH)_x]^{2-x+}$). Moreover, recent density functional theory (DFT) calculations by Van der Mynsbrugge et al. for Pd/H-CHA have inferred that Pd^+ ions are thermodynamically preferred over Pd^{2+} in some configurations [22]; for example, next-nearest neighbor (NNN) Al pairs (separated by a single Si atom) in the CHA 6-ring cannot provide the ideal square planar coordination to stabilize Pd^{2+}, such that the relative stability of Pd^+ and Pd^{2+} cations at these Al pairs depends on the temperature and partial pressure of water [22].

In addition to Pd^+ and Pd^{2+} ions, the presence of $[Pd(OH)]^+$ moieties in Pd zeolites has been inferred [11,15,16,23]. NO adsorption on $[Pd(OH)]^+$ is proposed to occur either via direct NO adsorption at the Pd center or via the reaction $NO + 2Z^-[Pd(OH)]^+ \leftrightarrow 2Z^-Pd^+ + NO_2 + H_2O$, where Z^- denotes a cation exchange site in the zeolite framework resulting from isomorphous substitution of Si by Al. In other words, $[Pd(OH)]^+$ is suggested to act as a precursor for the formation of Pd^+ ions [23–25]. However, the role of $[Pd(OH)]^+$ as sites for NO adsorption has been called into question by several groups [22,26]. DFT calculations indicate that $[Pd(OH)]^+$ is thermodynamically less stable than Pd^+/H^+ and Pd^{2+} at paired Al sites, and that under realistic experimental conditions the reaction of $[Pd(OH)]^+$ with adjacent protons to form Pd^{2+} and water is favorable [22]. The stability of Pd^{2+} and $[Pd(OH)]^+$ relative to non-exchanged species (solid Pd or PdO) has not been reported but can readily be calculated by combining the stability of exchanged Pd species relative to monoatomic Pd gas calculated by DFT with known free energies of formation for solid Pd and PdO versus Pd gas. For example, in 20 kPa O_2 and 5 kPa O_2, the free energies of $[Pd(H_2O)_4]^{2+}$, $Pd^+H^+(H_2O)_2$, and $Pd(OH)^+H^+$ at next-next-nearest neighbor Al pairs in a 6-membered ring are − 351, − 265, and − 177 kJ/mol versus atomic Pd at 300 K [22] compared to − 339 kJ/mol for metallic Pd and − 505 kJ/mol for PdO, indicating bulk PdO is the preferred phase at ambient temperature. At 1050 K, the free energies for Pd^{2+}, Pd^+H^+, and $[Pd(OH)]^+H^+$ at the same site are − 263, − 171, and − 25 kJ/mol relative to atomic Pd, and those of solid Pd and PdO are − 246 and − 249 kJ/mol respectively. High temperatures thus stabilize exchanged Pd at a subset of zeolite sites and lower the free energy penalty for exchange at all sites relative to non-exchanged bulk Pd phases. The free energy of exchanged Pd may be further lowered by as much as 80 kJ/mol upon adsorption of NO [17].

From the foregoing, the available evidence points towards Pd^+/H^+ and Pd^{2+} being the main sites involved in NO adsorption; in order to maintain charge balance, such species can form only at paired framework Al sites. In principle, Pd^+ or $[Pd(OH)]^+$ ions can additionally exist at isolated Al sites, providing a pathway exists for their formation from the Pd^{2+} precursor used for catalyst preparation. In this regard, it is of note that Van der Mynsbrugge et al. have reported that the NH_3 contained in the typical Pd precursor $Pd(NH_3)_4(NO_3)_2$ should be capable of driving the reduction of Pd^{2+} to Pd^+ upon insertion in H-CHA based on the calculated free energy of reaction [22]. The same authors also reported DFT calculations showing that the formation of Pd^+ is thermodynamically preferred to $[Pd(OH)]^+$ at isolated Al sites. Lardinois et al. found that CHA samples synthesized purposefully to contain no paired framework Al sites were able to stabilize 0.08 isolated Pd cations per Al, and proposed that the Pd species was $[Pd(OH)]^+$ based on the presence of an OH stretching feature at 3660 cm^{-1} in IR spectra and H_2 consumption per Pd of approximately 1.0 [11]. Notably, CHA samples containing significant amounts of six-membered ring (6-MR) paired Al sites, as quantified by Co^{2+} titration, were exchanged with Pd^{2+} and did not show the 3660 cm^{-1} IR feature, suggesting the preferential formation of Pd^{2+} at 6-MR paired Al sites. Moreover, at similar bulk Pd contents, the amount of isolated Pd sites formed on Pd-CHA samples systematically increased with their paired Al content, consistent with thermodynamic calculations that $(Z^-)_2Pd^{2+}$ sites are more stable than $Z^-[PdOH]^+$ after the high temperature air treatments required for the dispersion of Pd in H-CHA [11,22].

In practice, it is found that the formation of high dispersions of Pd cations at industrially relevant Pd loadings (≥1 wt%) requires a high framework Al content [27], which on average results in a high concentration of paired Al sites. Increasing the Al content inevitably decreases the hydrothermal stability of the zeolite; hence, the Si/Al ratio should be optimized while maximizing the percentage of paired Al sites for that Al content. The use of high calcination temperatures (≥650 °C) to ensure adequate mobility of the Pd species resulting from thermal decomposition of the Pd precursor is also a pre-requisite [11,12]. Given that increasing the amount of paired Al sites in the zeolite is beneficial for increasing the Pd dispersion, it follows that it is also beneficial for the NO storage capacity and that the NO/Pd ratio will tend towards unity as the Pd dispersion tends towards 100% [27]. Beyond this, however, it is unclear as to what effect increasing the amount of paired Al sites – at fixed Si/Al ratio – has on the NO adsorption properties of Pd/H-CHA under working conditions. Consequently, this study sought to examine the effect of the degree of Al pairing in Pd/H-CHA at fixed Si/Al ratio and Pd loading on PNA performance. The use of realistic exhaust conditions was emphasized given the known susceptibility of Pd-CHA to deactivate in the presence of CO [28–30] and the possible influence of Al site pairing on such catalyst deactivation and potential catalyst regeneration by means of high temperature oxidative treatment.

2. Materials and methods

2.1. Catalyst synthesis

CHA zeolites were hydrothermally synthesized following previously reported procedures [31,32] using Ludox AS-40 as the silica source. The other chemicals used in the synthesis were aluminum hydroxide (98%, SPI Pharma), aluminum isopropoxide (98%, Sigma-Aldrich), trimethyladamantylammonium hydroxide ($TMAda^+$, 25 wt% in water, Sachem), sodium hydroxide (98% Alfa Aesar) and deionized water (18.2 MΩ) (see Table S1 in Supplementary Information for the composition of the synthesis solutions). Zeolite synthesis solutions were homogenized for 2 h under ambient conditions and the solutions then transferred to Teflon-lined, stainless-steel autoclaves (Parr Instruments), sealed under autogenous pressure, and placed in a forced convection oven controlled to 160 °C for 6 days. The solid product was isolated by filtration on a Buchner funnel and washed thoroughly with deionized water, using a volume of water equivalent to five times that of the synthesis solution. The product was dried at 90 °C overnight and then calcined in flowing air according to the schedule shown in Table S2.

Zeolite samples were converted to their NH_4-form by stirring with 1 M of NH_4NO_3 (99.9 wt%, Sigma-Aldrich) at a ratio of 100 g of solution (g solid)$^{-1}$ under ambient conditions for 24 h. NH_4-form zeolites were recovered by centrifugation, washed with deionized water (30 mL (g solid)$^{-1}$ per wash) until the pH of the supernatant was constant, dried in a vacuum oven at 60 °C overnight, and then stored under an ambient atmosphere in capped borosilicate scintillation vials.

Pd-exchanged samples were prepared via incipient wetness impregnation. First, deionized water was added dropwise to NH_4-form zeolites while stirring with a plastic spatula until saturation of the total pore volume, evidenced by transformation from a free-flowing powder to a sticky solid. Assuming the same mass saturation point as pure water, aqueous $Pd(NH_3)_4(NO_3)_2$ (Sigma-Aldrich) solutions were appropriately diluted with deionized water and added dropwise to NH_4-form zeolites

while stirring to achieve a target Pd loading of 1 wt%. As-exchanged Pd-zeolite samples were left under ambient conditions overnight after which the zeolite was dried in a vacuum oven at 60 °C overnight, followed by calcination at 650 °C for 4 h in flowing air.

In order to prepare samples for evaluation, the Pd-CHA powders were washcoated onto cordierite monolith cores (400 cpsi/6.5 mil). Aqueous Zr acetate solution was used as a binding agent (ca. 3.5%), the content of Pd-CHA powder in the aqueous washcoat slurry in each case being targeted at ~35%. The slurry was agitated with a high shear mixer at 1400 rpm overnight and then manually coated onto 1″ x 3″ (d x l) monolith cores by dipping (1 min). Excess slurry was then removed by blowing compressed air through the monolith cores, which were then allowed to stabilize at room temperature for 2 h. The coated monoliths were dried in a static oven at 110 °C overnight, the washcoating being repeated until the target loading of ~115 g/l was reached. Finally, the washcoated cores were calcined at 550 °C (~1 °C min^{-1}) for 2 h in flowing air in a horizontal tube furnace.

2.2. Catalyst characterization

The zeolite framework topologies were characterized ex-situ by powder X-ray diffraction (XRD) using a Rigaku SmartLab X-ray diffractometer (Cu Kα radiation source, XRD patterns in SI). Zeolite powders (ca. 0.01 g) were lightly pressed with a microscope slide onto a low-dead-volume sample holder (Rigaku). XRD patterns were collected over a range of 4 − 40° 2θ with a 0.01° step size and a scan rate of 0.0167° s^{-1}.

The micropore volumes of the samples were determined via N_2 physisorption using a Micromeritics ASAP 2020 surface area and porosity analyzer. H-form and Pd-H form zeolites were evacuated under dynamic vacuum (5 μm Hg) and heated at 160 °C for 16 h prior to adsorption measurements. Volumetric uptakes of adsorbates between 0.10 and 0.20 P/P_0 were linearly extrapolated to zero relative pressure to estimate the micropore volume.

The number of 6-MR paired Al sites in CHA samples was quantified by Co^{2+} titration [31,33]. NH_4-form zeolites (10 g) were stirred with 1 M of $CoCl_2$ (150 mL, 98 wt%, Sigma-Aldrich) using a magnetic Teflon stir bar for > 8 h at 80 °C to achieve saturation. After exchange, the Co-exchanged zeolites were recovered by vacuum filtration, washed with water four times (30 mL (g solid)$^{-1}$ per wash), and dried in a static oven at 140 °C before treatment in flowing air at 600 °C for 1 h.

Elemental compositions were determined using X-ray fluorescence and inductively coupled plasma optical emission spectroscopy (ICP-OES). For ICP-OES characterization, samples (ca. 0.03−0.05 g) were digested in 2.5 g of hydrofluoric acid (48 wt%) for at least 3 days before diluting with 50 g of deionized water under ambient conditions. Digested samples were further acidified with 2.5 g of nitric acid (75 wt %) within a day of ICP-OES characterization. The Si/Al ratios of the solids were estimated by subtracting the contribution of extra framework cations and assuming a molar composition of $Si_{(1-x)}O_2Al_x$.

H_2 temperature programmed reduction (H_2 TPR) experiments were performed with a Micromeritics Autochem II 2920 Chemisorption Analyzer. An isopropanol slurry (−89 °C) was inserted just before the internal thermal conductivity detector (TCD) to trap any condensable gases (e.g., water). The TCD was calibrated using varied pressures (0.5−5 kPa) of H_2 in balance Ar, resulting in a response factor that quantified a Micromeritics supplied Ag_2O H_2 TPR standard within 11%. To characterize the Pd speciation, Pd-exchanged CHA zeolites (0.04−0.08 g) were dehydrated in flowing air (30 cm^3 min^{-1}) to 650 °C for 1 h before cooling to ambient temperatures. Samples were then treated in a flowing (30 cm^3 min^{-1}), wetted (1−3 kPa H_2O) Ar stream for at least 30 min. After removing water from the Ar stream and lowering the flowrate to 10 cm^3 min^{-1}, samples were cooled to −70 °C using a Micromeritics Cryocooler II accessory. The Ar stream was replaced with 5 kPa H_2 in balance Ar (10 cm^3 min^{-1}) and treated to 300 °C (10 °C min^{-1}). The assignment of temperature reduction features is discussed elsewhere [11].

In situ diffuse reflectance infrared Fourier transform spectroscopy (DRIFTS) measurements were carried out using a Harrick scientific praying mantis cell outfitted with a high temperature reaction chamber as described previously [16]. Samples were pretreated in Ar (dried by −78 °C cold trap) at 500 °C for 1 h prior to exposure to 1000 ppm CO in Ar (50 sccm) for 10 min at 25 °C.

2.3. Simulated cold start experiments

Fresh 1″ x 1″ monolithic core samples were evaluated for NOx storage and release performance on rapid temperature ramps performed on an automated flow reactor. The flow rate was 6.4 L min^{-1}, resulting in a gas hourly space velocity (SV) of 30 K h^{-1}. The feed gas always contained 120 ppm NO, 5 % H_2O, 5 % CO_2, 10 % O_2, and balance N_2 to simulate the exhaust conditions on a diesel engine operating at a lambda of 2.0. To evaluate the effects of the exhaust reductants on the NOx storage performance, tests were also performed with the feed gas composition above supplemented with 140 ppm C_2H_4, with 1350 ppm CO/450 ppm H_2, or with 140 ppm C_2H_4 + 1350 ppm CO/450 ppm H_2. With the oven temperature at 70 °C, the exhaust was directed through a bypass line to measure the feed gas concentrations for 240 s. Then the exhaust was redirected through the sample, and the oven immediately starting heating from 70 °C to 353 °C at the maximum ramp rate of the oven (1.4 °C/s). The bed temperature of the sample started each test at approximately 90 °C and reached a maximum near 550 °C. The catalyst was tested multiple times with each exhaust composition to simulate consecutive cold starts on a vehicle. After each test, the sample was cooled in 5% H_2O, 5% CO_2, 10% O_2, and balance N_2 to prepare for the next test. Before each test sequence with a different feed gas composition, the sample was exposed to 750 °C for approximately 1 h to ensure that the catalyst always began the test sequence in a similar and highly oxidized state.

To obtain an initial assessment of the thermal durability of each catalyst, the sample was exposed to 2 h at 600 °C in flowing exhaust gas with 5 % H_2O, 5 % CO_2, 10 % O_2, and balance N_2. The catalyst was then evaluated with the different exhaust compositions described above. The tests were also performed after the sample was exposed to an additional 2 h at 650 °C, after an additional 2 h at 700 °C, and after an additional 2 h at 750 °C.

Since the Pd loading was approximately 25% lower for Pd-CHA-2 than for the other two samples, the measured NOx storage capacities were normalized by the wt% Pd in the samples.

2.4. Catalyst evaluation in engine exhaust

Evaluation of the catalyst performance in the engine exhaust was conducted on a lean gasoline engine research platform installed in an engine test cell at Oak Ridge National Laboratory. A 4-cylinder 2.0-liter naturally aspirated direct-injection gasoline engine was used, originating from a European Model Year 2008 BMW 1-series 120i vehicle. The engine was coupled to a motoring dynamometer that controlled the engine speed and load. An EEE-lube certification gasoline fuel containing low sulfur levels (<8 ppm) was used to fuel the engine. Additional details on the engine platform and performance characteristics can be found in prior publications [34–36].

To accommodate testing of the core samples, a slipstream setup was employed where a portion of the engine exhaust was extracted and routed to a catalyst core sample via heated lines. A catalyst sample (D x L = 2 cm × 7.5 cm monolith) was placed inside the furnace, which was used to control the catalyst temperature. The flow through the reactor was adjusted by a needle valve installed downstream of the flow reactor and upstream of the heated sampling pump. A nominal flow rate of 11.8 liters per minute was controlled to achieve a 30,000 h^{-1} space velocity (SV) through the core samples. The effluent exhaust was directed to a MKS 2030-HS Fourier-Transform Infrared Spectrometer (FTIR) and

California Analytical Heated Flame Ionization Detection (HFID) Analyzer for real time analysis of gas species. The catalyst temperature was monitored with Type K thermocouple probes inserted at the catalyst inlet, middle and outlet locations. The engine and slip-stream setup are shown in Fig. S1.

Prior to the evaluations, all samples were degreened at 700 °C inlet temperature for 4 h on a synthetic exhaust flow reactor under neutral conditions (10% CO_2, 10% H_2O, balance N_2) according to the catalyst test protocol developed by the Advanced Combustion and Emissions Control Technical Team [37]. The degreened samples were then transferred to the engine laboratory for evaluation.

The evaluations were performed by extracting exhaust from the engine operating at 2000 rpm speed and 50 Nm load in the lean stratified combustion mode. The average exhaust concentrations are listed in Table 1.

Similar to the flow reactor studies, the measured NOx capacities from the engine tests were normalized by the weight percent of Pd in the samples.

3. Results and discussion

3.1. Catalyst synthesis and characterization

To facilitate studies assessing the effect of Al site pairing on the NO adsorption properties of Pd-CHA, three CHA samples were prepared containing approximately the same Si/Al ratio but differing fractions of paired Al sites. The preparations followed synthetic strategies previously reported by Di Iorio and Gounder [31,33], and the synthesis recipes are reported in Table S1 in the Supporting Information. X-ray diffractograms of the resulting samples, denoted as CHA-1, CHA-2 and CHA-3, are shown in Fig. S2, and confirm that the zeolites possess the intended chabazite topology. The results of N_2 physisorption are summarized in Table S3 and are consistent with the preparation of microporous materials. Elemental analysis data for the three samples are summarized in Table 2 and show that the Si and Al contents of the zeolites were similar, such that the molar Si/Al_2 ratios spanned a narrow range (19.0–20.8). After loading with Pd, the pore volumes of the zeolites in all cases decreased, suggesting that some degree of occlusion of the pores may have occurred, for example, as a result of PdO particle formation. As shown in Table S3, Pd loadings were similar for Pd-CHA-1 and Pd-CHA-3 (0.90 and 0.92 wt%, respectively), while the loading for Pd-CHA-2 was determined by ICP-OES to be 0.68 wt%.

The CHA-1 material was synthesized with only the organic structure-directing agent (SDA) $TMAda^+$ (i.e., Na^+-free) with the expectation of minimizing the formation of Co^{2+}-titratable framework Al pairs, which correspond to 2 Al atoms substituted in the 6-MR of CHA [33]. Consistent with previous reports [31,33], the CHA-1 material contained the lowest number of Al pairs for all zeolite samples with 6.5 % Al in pairs (Table 2). The CHA-2 sample was synthesized with the same Al precursor as CHA-1 (i.e., $Al(OH)_3$), but with both $TMAda^+$ and Na^+ as co-SDAs, and resulted in the greatest number of paired Al sites of all samples with 53% of Al in pairs (Table 2). The final sample, CHA-3, was synthesized with similar Na^+ and TMAdaOH contents as CHA-2, but instead the $Al(OH)_3$ precursor was replaced with an equivalent molar amount of Al isopropoxide. The CHA-3 material contained a lower amount of paired Al sites (10.8%) than CHA-2 (Table 2), which was inconsistent with previous reports that replacing $Al(OH)_3$ with Al isopropoxide resulted in a greater amount of Al pairs. Although the same synthesis gel molar compositions were used by Di Iorio and Gounder, the zeolite syntheses performed in this study occurred at larger scale (e.g., 50 g batches) than in lab-scale syntheses (e.g., 5 g batches), and other lurking variables such as the crystallization time likely influenced the degree of Al pairing in the final materials. Nonetheless, the three samples obtained showed different degrees of Al pairing (Table 2), which allowed subsequent studies of the role of Al pairing on Pd-CHA performance for PNA applications.

Table 1
Lean exhaust composition at 2000 rpm and 50 Nm lean stratified engine operation.

λ	NO (ppm)	NO_2 (ppm)	NOx (ppm)	CO (ppm)	THC (ppm)	CO_2 (%)	H_2O (%)	O_2 (%)
1.60	358	49	407	2422	811	8.3	9.5	7.6

H_2-TPR has previously been shown to be a powerful tool for characterizing the amount and identity of the Pd species (i.e., exchanged Pd cations or agglomerated PdO domains) in Pd-exchanged zeolites [11]. Typically, such TPR profiles contain three main features, namely, (i) a low temperature event (< 10 °C) corresponding to desorption of adsorbed Ar within the zeolite micropores, (ii) a feature near 10–75 °C corresponding to the reduction of agglomerated PdO particles, and (iii) a higher temperature feature (~75–180 °C) associated with the reduction of hydrated Pd cations. Fig. 1 displays the H_2-TPR profiles of CHA-1, CHA-2 and CHA-3 after loading with ~1 wt% Pd (confirmed by ICP analysis, Table S3, SI) and treatment in air to 650 °C (10 °C min^{-1}). Hereafter, these samples are referred to as Pd-CHA-1, Pd-CHA-2 and Pd-CHA-3. In the case of Pd-CHA-2 and Pd-CHA-3, the lack of a reduction event in the 10–75 °C range is consistent with the absence of significant amounts of agglomerated PdO. In contrast, Pd-CHA-1 is characterized by a well-defined reduction event centered at ~50 °C, evincing the presence of PdO. Integration of the Pd reduction features for Pd-CHA-1 suggested that just over one-third of the Pd is present at PdO, the remainder corresponding to mononuclear Pd^{2+} species. As shown in Table 2, CHA-1 contained the lowest amount of paired Al sites in the three samples, such that the theoretical maximum Pd loading attainable at the paired sites corresponds to 0.55 wt%, which is lower than the actual Pd loading of 0.9 wt% used. Hence, these results are consistent with the inability of the zeolite framework in CHA-1 to charge compensate all of the loaded Pd^{2+} ions, resulting in PdO formation. In the case of Pd-CHA-3, the maximum Pd loading attainable at the paired sites is calculated to be 0.85 wt%. This is evidently sufficiently close to the actual Pd loading of 0.92 wt% that significant formation of PdO is not observed. Moreover, as noted in the Introduction, Lardinois et al. [11] have reported that CHA samples containing no 6-MR paired Al sites (Co^{2+}/Al < 0.01) are able to stabilize 0.08 mononuclear Pd^{2+} per Al, indicating that isolated Al sites can stabilize isolated Pd^{2+} sites to a limited degree; such sites are proposed to be $Z^-[Pd(OH)]^+$. Hence, a perfect correlation between the concentration of paired Al sites and the maximum concentration of isolated Pd species that can be attained cannot be expected.

CO-DRIFTS measurements were also used to characterize the Pd-exchanged samples, the results being collected in Fig. S3 and Table S4. All three samples exhibited CO-DRIFTS spectra broadly typical of Pd-CHA [18], although differences in the spectra indicate that the Pd speciation differs between the three materials. Pd-CHA-1 exhibited the weakest Pd-CO band intensity, consistent with the fact that it contained comparatively more PdO and a lower proportion of cationic Pd species than the other two samples. In the case of Pd-CHA-2, the $[Pd(CO)OH]^+$ band at 2127 cm^{-1} – observed for Pd-CHA-1 and -3 – was largely absent, suggesting that $[Pd(OH)]^+$ species are less prevalent in this sample. In the case of Pd-CHA-3, the Pd-CO spectral features are essentially a mix of the other two samples.

3.2. Effect of paired aluminum sites on repeated simulated cold starts

3.2.1. Laboratory assessment of Pd-CHA-1 without reductants and with C_2H_4

The fresh Pd-CHA-1 sample was evaluated on three consecutive temperature ramp tests without reductants followed by five consecutive tests with 140 ppm C_2H_4. Fig. S4 shows the measured NOx slip from the catalyst during these tests. Representative traces of the inlet and bed temperatures are also included in the figure. The NOx slip results were

Table 2
Analytical data for CHA samples varying in paired Al content, including elemental analysis and Co^{2+} titration.

Sample	Si (wt %)	Al (wt %)	Si/Al_2 (molar)	Co (wt %)	Co/Al (molar)	Al at paired sites (wt%)	Al at isolated sites (wt%)	Normalized max. Pd^{2+} at paired Al sites (wt%)	Comment
CHA-1	42.68	4.31	19.0	0.308	0.033	0.28	4.03	0.55	6.5 % of Al paired
CHA-2	42.1	3.89	20.8	2.25	0.265	2.06	1.83	3.99	53.0 % of Al paired
CHA-3	42.87	4.02	20.5	0.475	0.054	0.43	3.59	0.85	10.8 % of Al paired

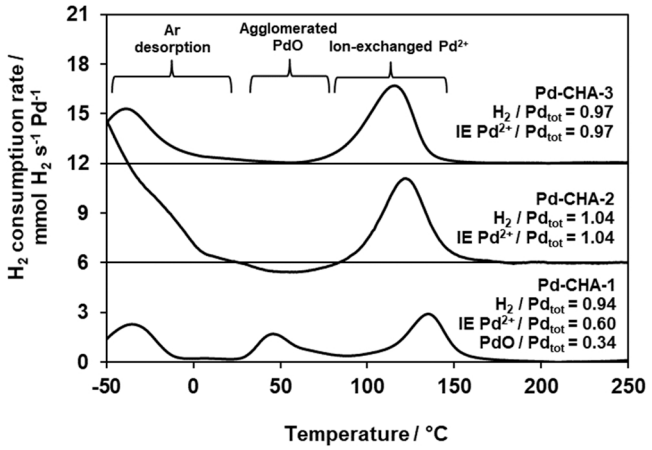

Fig. 1. H_2 temperature programmed reduction profiles of Pd-CHA-1, Pd-CHA-2 and Pd-CHA-3 after treatment in air at 650 °C.

very consistent from run to run without C_2H_4 as well as with C_2H_4, suggesting that the catalyst structure was stable during the tests. The presence of C_2H_4 significantly improved the NOx storage capability of the catalyst for the initial 100 s of the tests, consistent with previous reports [30,38,39]. The catalyst began to release the stored NOx when the NOx slip exceeded the feed gas NO level. This occurred at a bed temperature of 212 °C without C_2H_4 and at 330 °C with C_2H_4. This suggests that the presence of C_2H_4 stabilized the stored NOx and delayed its release by over 100 °C. Finally, the amount of NOx released was significantly higher with C_2H_4, verifying that more NOx had been stored on the tests with C_2H_4.

As further evidence that the presence of C_2H_4 stabilized the stored NOx to higher temperatures, Fig. S4 indicates that the NOx slip consistently dropped below the feed gas NO level as the bed temperature dropped from the maximum bed temperature of 555 °C during the tests with C_2H_4 but not on the tests without reductants. N_2O and NH_3 formation were insignificant on the tests with C_2H_4, suggesting that this drop in NOx slip at the end of the tests was due to NOx storage and not due to NOx reduction by C_2H_4 (i.e., hydrocarbon SCR).

The NOx slip data was used to calculate the cumulative amount of NOx stored in the sample as a function of time during a test. Fig. S5 shows the cumulative amount of stored NOx (normalized by the volume of the sample) for the 3 tests without C_2H_4 and the 5 tests with C_2H_4. With and without C_2H_4, the cumulative amount of stored NOx returned to zero when the bed temperature reached 555 °C, indicating that all of the stored NOx had been released. On the tests with C_2H_4, however, the cumulative amounts began to increase again as the temperature dropped from 555 °C and the sample started storing NOx again. Fig. S5 indicates that the maximum amounts of stored NOx were between 0.20 and 0.22 g/L on the tests with C_2H_4 and near 0.12 g/L on the tests without C_2H_4. Hence, the presence of C_2H_4 increased the maximum amount of stored NOx by 65–80%.

To provide an initial assessment of the thermal durability of Pd-CHA-1, a second sample was evaluated for fresh NOx storage performance on multiple tests with and without 140 ppm C_2H_4. It was similarly tested after 2 h at 600 °C and after 2 additional h at 650 °C, 700 °C, and 750 °C. Fig. S6 shows the maximum NOx storage capacities (from the cumulative NOx plots) with and without C_2H_4 as a function of the run number for the different aging conditions. For all aging conditions, the presence of C_2H_4 significantly increased the maximum NOx capacity. The maximum capacities were consistent from run to run on the tests without C_2H_4, but the capacities dropped modestly from run to run on the tests with C_2H_4. For example, the maximum capacity of the sample aged 2 h at 750 °C dropped by approximately 14% over 21 tests. With and without C_2H_4, Fig. S6 shows that the maximum capacities dropped incrementally as the aging temperature increased, which can be attributed to thermal degradation of the sample.

3.2.2. Comparison of Pd-CHA-1, Pd-CHA-2, and Pd-CHA-3 without and with C_2H_4

The fresh Pd-CHA-2 and Pd-CHA-3 samples were also evaluated on multiple NOx storage tests with and without C_2H_4. Fig. 2 compares the maximum NOx storage capacities of the three samples normalized by the Pd loading. The maximum NOx capacity of all three samples was relatively consistent from run to run without C_2H_4, but there was a modest drop in NOx capacity on the tests with C_2H_4. Without C_2H_4, the maximum normalized capacities followed the ordering Pd-CHA-2 > Pd-CHA-3 > Pd-CHA-1, i.e., the same ordering as the concentration of paired Al sites in the samples. With C_2H_4, Pd-CHA-2 and Pd-CHA-3 showed similar NOx storage capacities, these being significantly higher than that of Pd-CHA-1 although the increase in capacity resulting from the presence of C_2H_4 was actually higher for Pd-CHA-3 than for Pd-CHA-2.

Similar to Pd-CHA-1, the Pd-CHA-3 sample was assessed with and without C_2H_4 after aging for 2 h at 650 °C, 700 °C, and 750 °C (note: Pd-CHA-3 was not exposed to 2 h at 600 °C). Fig. 3 compares the maximum

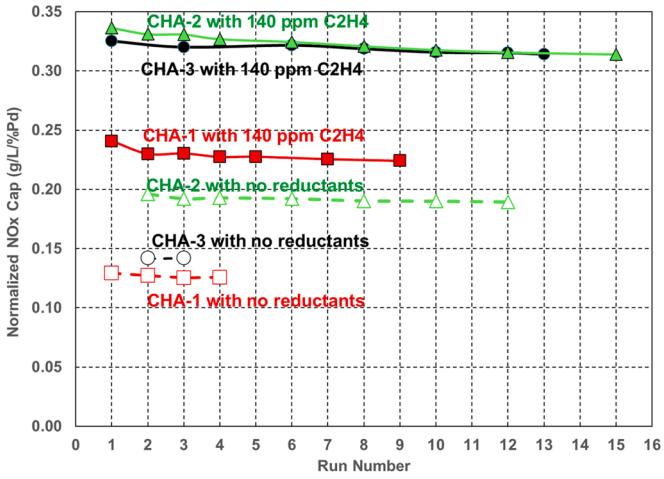

Fig. 2. Maximum normalized NOx storage capacities for fresh Pd-CHA-1, Pd-CHA-2, and Pd-CHA-3 on temperature ramp tests with 110 ppm NO, 5 % H_2O, 5 % CO_2, 10 % O_2, with and without 140 ppm C_2H_4. NOx storage capacities were normalized by the Pd loading.

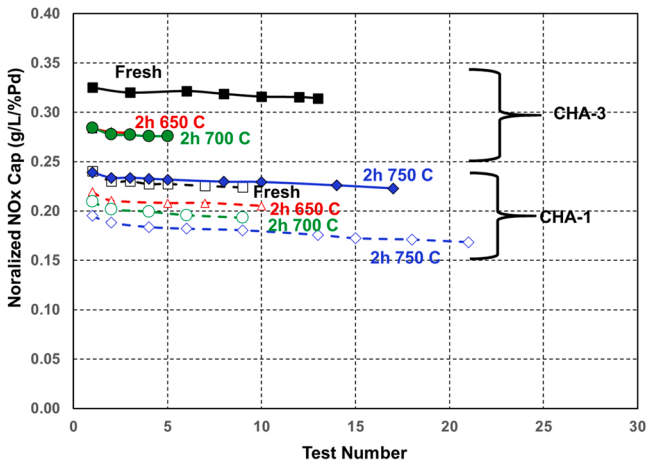

Fig. 3. Maximum normalized NOx storage capacities for second sample of Pd-CHA-1 (solid lines, closed symbols) and for Pd-CHA-3 (dashed lines, open symbols) on temperature ramp tests with 110 ppm NO, 5 % H_2O, 5 % CO_2, 10 % O_2, and 140 ppm C_2H_4 for fresh catalysts and after 2 h exposures to 650 °C, 700 °C, and 750 °C.

normalized NOx storage capacities with C_2H_4 for Pd-CHA-1 and Pd-CHA-3 after the different thermal treatments. Like Pd-CHA-1, the capacity of Pd-CHA-3 decreased gradually on the consecutive tests with C_2H_4 after exposure to 2 h at 750 °C. However, Pd-CHA-3 appeared to be less susceptible to deactivation, as it only lost 7 % of its capacity over 17 tests, compared to a loss of 13% over 18 tests for Pd-CHA-1. Similar to Pd-CHA-1, Pd-CHA-3 gradually lost NOx storage capacity as the aging temperature increased.

Fig. 4 shows the corresponding data for the fresh Pd-CHA-2 and after 2 h exposures to 600 °C, 650 °C, 700 °C, and 750 °C. In contrast to Pd-CHA-1 and more like Pd-CHA-3, the NOx capacity of Pd-CHA-2 was relatively consistent from test to test on the consecutive tests with C_2H_4 after exposure to 2 h at 750 °C, as Pd-CHA-2 lost about 7 % of its capacity over 10 tests. In contrast to Pd-CHA-1 in Fig. S6, the capacity of Pd-CHA-2 was much more thermally robust on the tests without C_2H_4, as the capacity remained essentially constant after the various aging temperatures. With C_2H_4, the NOx capacity was constant after exposures to 600 °C and 650 °C and actually increased after exposures to 700 °C and 750 °C. This increase after the higher temperature exposures may have been due to better exchange of the Pd within the chabazite zeolite. Since Pd-CHA-2 had the highest percentage of paired Al sites, the data suggest that this may have been beneficial for the thermal durability of the catalyst.

The normalized NOx capacities of the fresh Pd-CHA-2 and Pd-CHA-3 with C_2H_4 were similar in Fig. 2. Since the maximum capacity of Pd-CHA-3 with C_2H_4 decreased after the 750 °C exposure while the capacity of Pd-CHA-2 increased after the 750 °C exposure, Pd-CHA-2 had significantly higher normalized NOx capacity after the thermal exposure (i.e., 0.35 g/L/%Pd vs 0.24 g/L/%Pd on the initial tests). Both of these samples had higher NOx capacities than the aged Pd-CHA-1 (0.20 g/L/%Pd), which had the lowest percentage of paired Al sites of the 3 samples. Altogether, these data suggest that a higher percentage of paired Al sites is beneficial for the NOx storage performance as well as the thermal durability of low temperature NOx adsorbers.

3.2.3. Comparison of Pd-CHA-1, Pd-CHA-2, and Pd-CHA-3 with CO/H_2

The greatest technical issue for LTNAs is the deactivation that has been observed on consecutive tests with high levels of CO/H_2 [30]. Therefore, the samples of Pd-CHA-1, Pd-CHA-2 and Pd-CHA-3 aged for 2 h at 750 °C were evaluated on multiple tests with 1350 ppm CO/450 ppm H_2. A second sample of Pd-CHA-2 that had been aged for 1 h at 750 °C was also assessed with the CO/H_2 mixture. Fig. 5 shows the results for the four samples. A comparison with the fresh data in Fig. 2 indicates that CO/H_2 increased the normalized NOx storage capacities of the samples on the initial tests following the 750 °C treatments. However, all four samples lost significant NOx storage capacity on the consecutive tests with the CO/H_2 mixture. This can be attributed to reduction of the Pd by the CO and was confirmed in the case of Pd-CHA-2 by the results of lean CH_4 light-off tests [30] performed after the consecutive NOx storage tests, the observed CH_4 light-off behavior of the spent catalyst being very similar to that after a rich reduction (see Fig. S7). The two samples of Pd-CHA-2 had similar normalized NOx storage capacities, and they were much higher than those of Pd-CHA-1 and Pd-CHA-3. This suggests that a higher percentage of paired Al sites is beneficial for the NOx storage performance with CO/H_2. Interestingly, Fig. 2 showed that the fresh Pd-CHA-3 and Pd-CHA-2 had similar normalized NOx storage capacity on tests with C_2H_4, although the improvement from C_2H_4 relative to the tests without reductants was actually larger for Pd-CHA-3. However, Pd-CHA-2 had significantly higher normalized NOx capacity than Pd-CHA-3 with CO/H_2 after the 2 h at 750 °C. Since Pd-CHA-2 had a larger percentage of paired aluminum sites and Pd-CHA-3 had a larger percentage of single aluminum sites, it can be speculated that CO can interact more

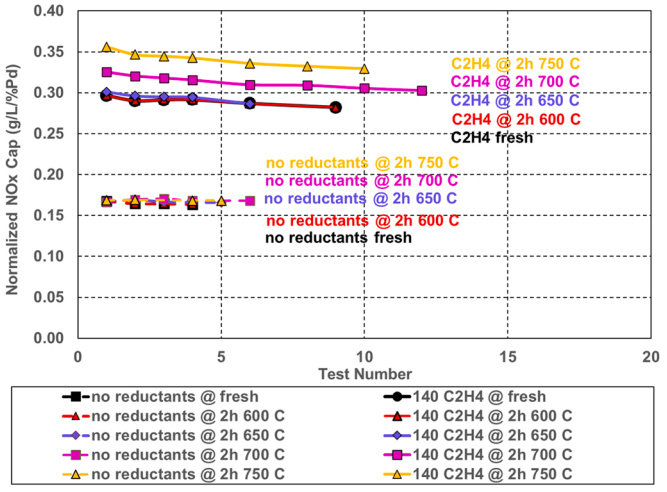

Fig. 4. Maximum normalized NOx storage capacities for Pd-CHA-2 sample on temperature ramp tests with 110 ppm NO, 5% H_2O, 5% CO_2, 10% O_2, with and without 140 ppm C_2H_4 for fresh catalyst and after 2 h exposures to 600 °C, 650 °C, 700 °C, and 750 °C.

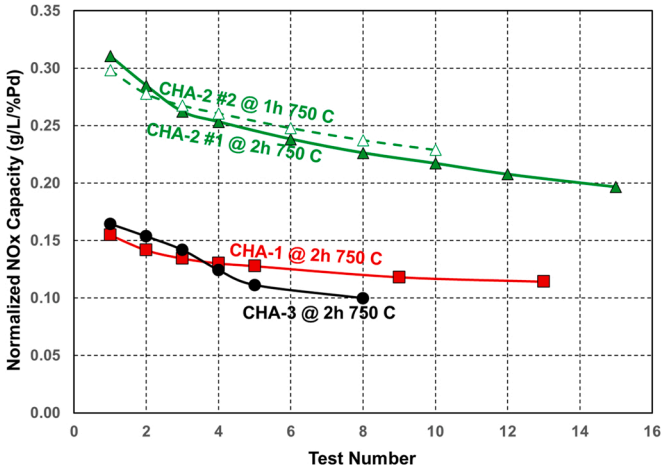

Fig. 5. Maximum normalized NOx storage capacities for Pd-CHA-1, Pd-CHA-3, and two samples of Pd-CHA-2 after aging up to 750 °C on temperature ramp tests with 110 ppm NO, 5% H_2O, 5% CO_2, 10% O_2, and 1350 ppm CO/450 ppm H_2. NOx storage capacities were normalized by the Pd loading.

effectively with Pd at paired aluminum sites by forming a $Pd(CO)(NO)^{2+}$ complex [40], while C_2H_4 can interact more effectively with Pd at single aluminum sites due to steric hindrance considerations.

3.2.4. Comparison of Pd-CHA-1, Pd-CHA-2, and Pd-CHA-3 with C_2H_4+CO/H_2

Diesel exhaust always contains a mixture of CO, H_2, and a wide variety of HC species. As a result, laboratory tests with both hydrocarbons and CO/H_2 in the feed gas are most representative. Therefore, the aged samples of Pd-CHA-1, Pd-CHA-3, and both samples of Pd-CHA-2 were evaluated on consecutive tests with 140 ppm C_2H_4 and 1350 ppm CO/450 ppm H_2 (note: the second sample of Pd-CHA-2 was exposed to another hour at 750 °C prior to these tests). Fig. 6 shows the normalized maximum NOx storage capacities of the four samples. Again, the capacities of all four samples dropped during the consecutive tests. Since C_2H_4 alone caused only a small loss in NOx capacity in Figs. 3 and 4, most of the deactivation in Fig. 6 can be attributed to the CO. The capacities of both samples of Pd-CHA-2 were nearly identical. While the Pd-CHA-2 samples did lose some NOx capacity, the loss was much less severe than that of Pd-CHA-1 and Pd-CHA-3. The higher percentage of paired aluminum sites in Pd-CHA-2 may have been beneficial for improving the robustness of the LTNA during consecutive tests with C_2H_4 and CO/H_2. It is possible that the Pd at single Al sites is more prone to being reduced to metallic Pd by the CO [30]. In contrast, the Pd at paired Al sites can form the $Pd(CO)(NO)^{2+}$ complex at low temperatures during tests with NO and CO [3,40]. After the stored NO and CO are released at higher temperatures, the Pd^{2+} is retained and remains unreduced.

3.3. Assessment of catalyst performance in engine exhaust

3.3.1. Effect of aluminum site pairing on NOx storage capacity

To assess the effects of the framework Al pairing on the NOx storage properties of the Pd-exchanged CHA core samples in actual engine exhaust and how they compare to results obtained in simulated exhaust, the three samples were evaluated in the gasoline lean engine exhaust using a slipstream setup. The cold-start NOx trapping efficiency of the Pd-CHA core samples was evaluated at 90 °C inlet temperature (set by the furnace) with the inlet exhaust gas composition listed in Table 1. Prior to the evaluation, each sample was pre-treated in the lean engine exhaust at 600 °C for 20 min. Following the pre-treatment, the sample was cooled down to 90 °C in room air. Once the temperatures stabilized, the exhaust was introduced to the sample via a switching valve.

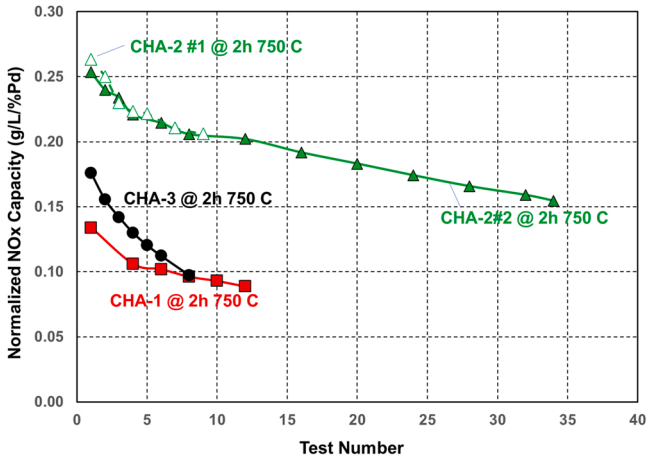

Fig. 6. Maximum normalized NOx storage capacities for Pd-CHA-1, Pd-CHA-3, and two samples of Pd-CHA-2 after aging 2 h at 750 °C on temperature ramp tests with 110 ppm NO, 5% H_2O, 5% CO_2, 10% O_2, 140 ppm C_2H_4, and 1350 ppm CO/450 ppm H_2. NOx storage capacities were normalized by the Pd loading.

The NOx adsorption profiles during the 90 °C storage phase are shown in Fig. 7a. The onset of the NOx slip was observed as soon as the catalysts were exposed to the exhaust. This can be partly attributed to the high feedgas NOx level of the engine exhaust. Pd-CHA-1 and Pd-CHA-3 exhibited similar NOx slip profiles. After the initial sharp increase in NOx slip, the NOx slip slowed down and reached feed levels within 60 s from the beginning of exhaust exposure, indicating that the catalysts became fully saturated. Much slower increase in NOx slip was observed on the Pd-CHA-2 sample, indicating much higher initial NOx storage capacity of the Pd-CHA-2 sample under the conditions studied here.

The integrated NOx storage capacities during isothermal adsorption were normalized by the percent Pd and are shown in Fig. 7b. Pd-CHA-2 demonstrated much higher NOx storage than Pd-CHA-3 and Pd-CHA-1, with Pd-CHA-3 storing slightly more than Pd-CHA-1. It appears that NOx storage scales with the amount of paired Al sites available in these samples since Pd-CHA-2 had a significantly higher percentage of paired Al sites than Pd-CHA-3 and Pd-CHA-3 had slightly more than Pd-CHA-1 (53.0%, 10.8% and 6.5% for Pd-CHA-2, Pd-CHA-3 and Pd-CHA-1, respectively; see Table 2). These results are consistent with the flow reactor observations suggesting that a higher percentage of paired Al sites is beneficial for increasing the NOx storage capacity of the Pd-exchanged CHA adsorbers.

3.3.2. Effect of NOx adsorption temperature

The effect of the adsorption temperature on the NOx trapping performance was assessed at 60 and 90 °C adsorption temperatures on Pd-CHA-2 and Pd-CHA-3 samples. At the 60 °C adsorption temperature, both samples exhibited similar NOx trapping performance as shown in Fig. 8, suggesting that at lower adsorption temperatures NOx trapping was mostly unaffected by the framework Al arrangement. As the adsorption temperature was increased to 90 °C, a significant increase in NOx trapping was observed on the Pd-CHA-2 sample, while the NOx storage of Pd-CHA-3 was mostly unchanged. At this temperature, Pd-CHA-2 stored almost three times as much NOx as Pd-CHA-3 on a normalized basis, clearly indicating the benefit of a higher percentage of paired Al sites for improving the NOx storage capacity under these adsorption conditions. The temperature effects observed here are most likely related to the Pd hydration/dehydration processes [41], the extent of which appears to be affected by the adsorption temperature and framework Al arrangement.

3.3.3. Effect of repeated simulated cold starts

It is now well established in the literature that the Pd-exchanged zeolites gradually lose NOx storage capacity over multiple consecutive storage and release cycles (representative of multiple cold-start events) due to the reduction of Pd by CO [30], which is one of the major durability concerns for practical applications. To assess if Al arrangement plays a role in improving the stability of the Pd-exchanged CHA adsorbers, the Pd-CHA-2 and Pd-CHA-3 samples were evaluated over multiple consecutive storage and release cycles. The experiments were carried out by exposing each sample to the engine exhaust at 60 °C during the storage phase, followed by a temperature ramp to 410 °C at 20 °C/minute and, after a cool down in room air, the cycle was repeated 4–6 times. Consistent with flow reactor results, both samples showed a decrease in NOx storage amount from test to test as shown in Fig. 9, but there was not a clear trend on whether the amount of paired Al sites improved the stability of the NOx storage performance during these consecutive cycles.

3.3.4. Effect of pre-treatment temperature

The decrease in NOx storage capacity observed over multiple consecutive storage and release cycles was found to be recoverable by pre-treating the samples in the lean exhaust at 600 °C for 20 min. During this pre-treatment, the temperature at the catalyst mid-bed location reached 660 °C. As shown Fig. 10, starting with the initial NOx storage

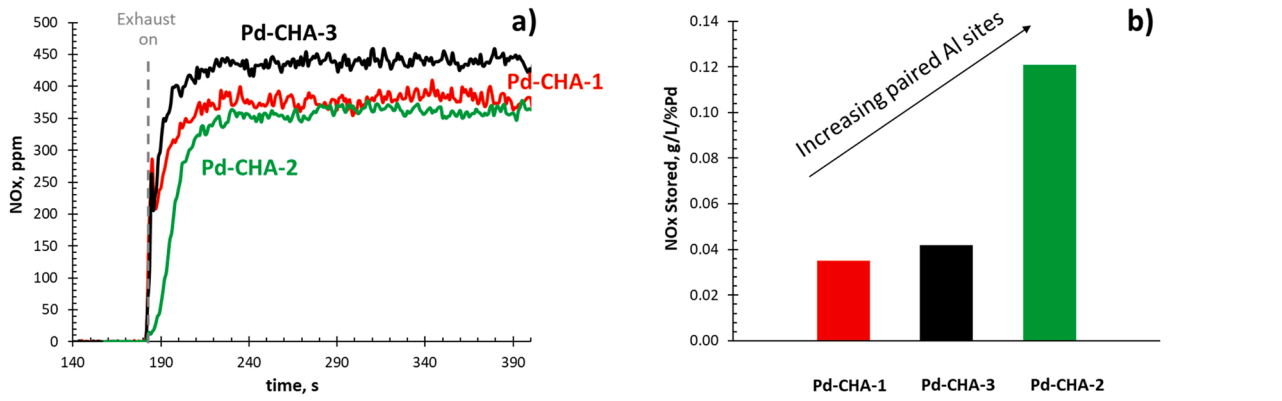

Fig. 7. a) NOx concentration profiles and b) total normalized NOx storage on Pd-CHA-1, Pd-CHA-2 and Pd-CHA-3 during 90 °C exposure to engine exhaust with compositions listed in Table 1.

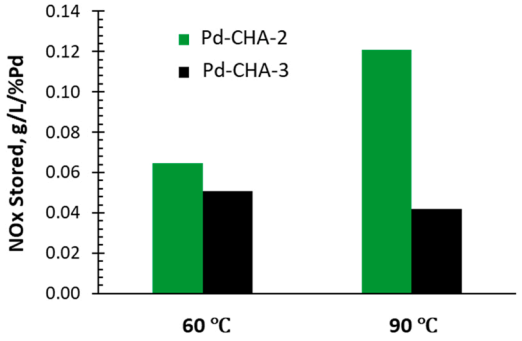

Fig. 8. Total normalized NOx storage capacities on Pd-CHA-2 and Pd-CHA-3 during 60 °C and 90 °C exposure to engine exhaust.

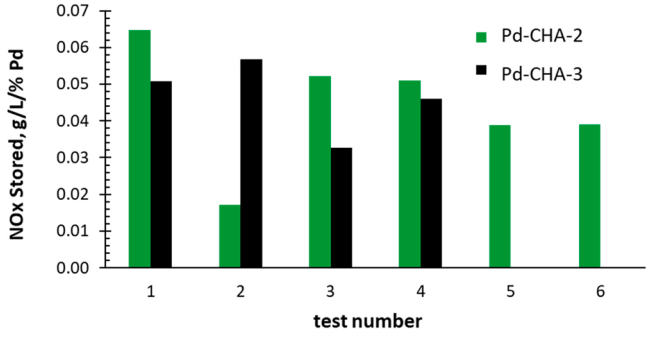

Fig. 9. Total normalized NOx storage capacities on Pd-CHA-2 and Pd-CHA-3 during multiple consecutive storage and release cycles. Each cycle consisted of a 60 °C storage phase followed by a temperature ramp to 410 °C at 20 °C min^{-1}.

capacity of 0.04 g/L, the normalized NOx storage capacity of Pd-CHA-3 decreases modestly from test to test (tests 2–4). However, after the sample was pre-treated again in the lean engine exhaust at 600 °C for 20 min, the original storage capacity was restored (test #5). It appears that this pre-treatment was sufficient to re-oxidize the Pd that was reduced during the consecutive cold-start tests. Interestingly, the NOx storage capacity significantly increased (more than 2x) after exposing the sample to lean exhaust at 700 °C (770 °C mid-bed temperature) for 20 min. This may be attributed to a re-dispersion of the Pd deeper within the zeolite after the high temperature exposure and, therefore, increasing the availability of the storage sites [11,12].

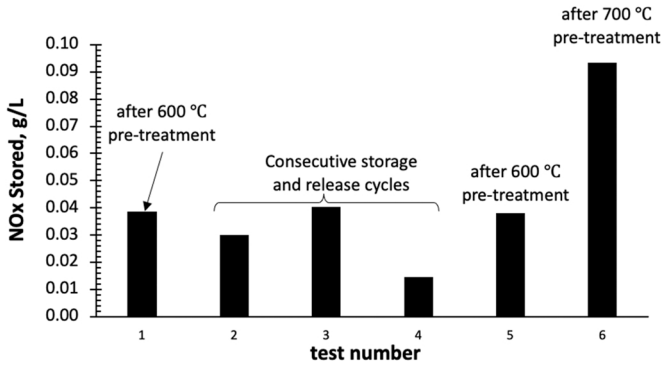

Fig. 10. Total NOx storage on Pd-CHA-3 during a 90 °C exhaust exposure after pre-treatments at 600 and 700 °C.

4. Conclusions

This work sought to assess the effect of Al pairing in Pd/H-CHA on the performance of this material as a passive NOx adsorber. According to the results of H_2 TPR, the two Pd/H-CHA samples with the highest concentration of paired Al sites (Pd-CHA-2 and Pd-CHA-3) contained Pd almost exclusively as isolated cations, whereas in Pd-CHA-1 PdO was also present. These results are consistent with the inability of the zeolite framework in Pd-CHA-1 to charge compensate all of the loaded Pd^{2+} ions. Given the inability of PdO to store NOx, Pd-CHA-1 consequently exhibited the lowest NOx storage capacity of the three samples in simulated cold start test performed with model diesel or actual lean gasoline exhaust gas. Pd-CHA-2 (containing 53% paired Al sites) displayed higher NOx storage capacity than Pd-CHA-3 (10.8% paired Al sites) during steady state adsorption tests with lean gasoline exhaust at 90 °C, and when tested under simulated cold start conditions using model diesel exhaust in the absence of reductants. Tests using model diesel exhaust incorporating ethylene boosted the storage capacity of all three samples, in line with previous reports for Pd-CHA. Curiously, this effect was most significant for Pd-CHA-3 when fresh; a clear explanation for this result is currently lacking, although one can speculate that it may reflect the ability of C_2H_4 to interact more effectively with Pd at single aluminum sites as opposed to paired Al sites due to steric hindrance considerations.

Notably, when tested with model diesel exhaust containing CO/H_2, Pd-CHA-2 showed significantly better storage capacity than Pd-CHA-1 and Pd-CHA-3, and deactivated less rapidly upon repeated cold start tests. This is a significant finding, given that CO-induced Pd reduction and sintering has been identified as the major deactivation pathway for Pd-zeolite PNAs. The reasons for the superior stability of Pd-CHA-2 can

be several fold, however, as noted earlier, DFT calculations by van der Mynsbrugge et al. show that Pd^{+}/Pd^{2+} species are thermodynamically more stable than $[Pd(OH)]^{+}$ species; hence, the latter species, which should occur in zeolites with mainly isolated Al sites, may be more prone to reduction by CO, although this remains to be proven. Moreover, given that increasing the amount of paired Al sites in the zeolite is beneficial for increasing the Pd dispersion, it follows that thermally-induced redispersion of formed PdO, which in principle can occur to some degree towards the end of cold-start temperature ramps, should be more facile for zeolites possessing a high concentration of paired Al sites.

Finally, Pd-CHA-1 and Pd-CHA-3 lost NOx storage capacity after exposure to high temperature treatments up to 750 °C, while the NOx capacity of Pd-CHA-2 actually increased upon exposure to 750 °C. This increase may have been due to better exchange of the Pd within the zeolite framework. These results suggest that a high concentration of paired Al sites can be beneficial for the thermal durability of the catalyst.

In summary, these results indicate that a high concentration of paired Al sites in Pd/H-CHA is beneficial for NOx storage capacity, thermal durability, and minimizing deactivation in the presence of CO/H_2.

CRediT authorship contribution statement

Joseph Theis: Conceptualization, Methodology, Validation, Investigation, Writing – original draft, Writing – review & editing. **Justin Ura:** Investigation, Validation. **Andrew Bean Getsoian:** Conceptualization, Methodology, Investigation, Writing – review & editing. **Vitaly Prikhodko:** Conceptualization, Methodology, Validation, Investigation, Writing – original draft, Writing – review & editing. **Calvin Thomas:** Investigation, Validation. **Josh Pihl:** Resources. **Trevor Lardinois:** Investigation, Validation. **Rajamani Gounder**: Conceptualization, Resources, Supervision, Writing – original draft, Writing – review & editing. **Xinyi Wei:** Investigation, Resources. **Yaying Ji:** Investigation. **Robert Pace:** Investigation. **Mark Crocker:** Conceptualization, Resources, Supervision, Writing – original draft, Writing – review & editing, Project administration, Funding acquisition.

Declaration of Competing Interest

The authors declare that they have no known competing financial interests or personal relationships that could have appeared to influence the work reported in this paper.

Data Availability

The authors do not have permission to share data.

Acknowledgements

This work was funded by the Department of Energy Office of Vehicle Technologies award number DEEE0008213. This report was prepared as an account of work sponsored by an agency of the United States Government. Neither the United States government nor any agency thereof, nor any of their employees, makes any warranty, express or implied, or assumes any legal liability or responsibility for the accuracy, completeness, or usefulness of any information, apparatus, product, or process disclosed, or represents that its use would not infringe privately owned rights. Reference herein to any specific commercial product, process, or service by trade name, trademark, manufacturer, or otherwise does not necessarily constitute or imply its endorsement, recommendation, or favoring by the United States government or any agency thereof. The views and opinions of authors expressed herein do not necessarily state or reflect those of the United States government or any agency thereof.

Appendix A. Supporting information

Supplementary data associated with this article can be found in the online version at doi:10.1016/j.apcatb.2022.122074.

References

[1] H.-Y. Chen, J.E. Collier, D. Liu, L. Mantarosie, D. Durán-Martín, V. Novák, R. R. Rajaram, D. Thompsett, Low temperature NO storage of zeolite supported Pd for low temperature diesel engine emission control, Catal. Lett. 146 (2016) 1706–1711.
[2] Y. Gu, W.S. Epling, Passive NOx adsorber: an overview of catalyst performance and reaction chemistry, Appl. Catal. A 570 (2019) 1–14.
[3] K. Khivantsev, F. Gao, L. Kovarik, Y. Wang, J. Szanyi, Molecular level understanding of how oxygen and carbon monoxide improve NOx storage in palladium/SSZ-13 passive NOx adsorbers: the role of NO^{+} and Pd-(II)(CO)(NO) species, J. Phys. Chem. C 122 (2018) 10820–10827.
[4] J.R. Theis, An assessment of Pt and Pd model catalysts for low temperature NOx adsorption, Catal. Today 267 (2016) 93–109.
[5] Y. Zheng, L. Kovarik, M.H. Engelhard, Y. Wang, Y. Wang, F. Gao, J. Szanyi, Low-temperature Pd/zeolite passive NOx adsorbers: structure, performance, and adsorption chemistry, J. Phys. Chem. C 121 (2017) 15793–15803.
[6] K. Khivantsev, N.R. Jaegers, L. Kovarik, S. Prodinger, M.A. Derewinski, Y. Wang, F. Gao, J. Szanyi, Palladium/Beta zeolite passive NOx adsorbers (PNA): clarification of PNA chemistry and the effects of CO and zeolite crystallite size on PNA performance, Appl. Catal. A Gen. 569 (2019) 141–148.
[7] J. Lee, Y. Ryou, A.J. Cho, H. Lee, C.H. Kim, D.H. Kim, Investigation of the active sites and optimum Pd/Al of Pd/ZSM−5 passive NO adsorbers for the cold-start application: evidence of isolated-Pd species obtained after a high-temperature thermal treatment, Appl. Catal., B 226 (2018) 71–82.
[8] B. Zhang, M. Shen, J. Wang, J. Wang, J. Wang, Investigation of various Pd species in Pd/BEA for cold start application, Catalysts 9 (2019) 247.
[9] R. Villamaina, U. Iacobone, I. Nova, E. Tronconi, M.P. Ruggeri, L. Mantarosie, J. Collier, D. Thompsett, Mechanistic insight in NO trapping on Pd/Chabazite systems for the low-temperature NOx removal from diesel exhausts, Appl. Catal. B Environ. 284 (2021), 119724.
[10] A. Wang, K. Lindgren, M. Di, D. Bernin, P.-A. Carlsson, M. Thuvander, L. Olsson, Insight into hydrothermal aging effect on Pd sites over Pd/LTA and Pd/SSZ-13 as PNA and CO oxidation monolith catalysts, Appl. Catal. B Environ. 278 (2020), 119315.
[11] T.M. Lardinois, J.S. Bates, H.H. Lippie, C.K. Russell, J.T. Miller, H.M. Meyer III, K. A. Unocic, V. Prikhodko, X. Wei, C.K. Lambert, A.B. Getsoian, R. Gounder, Structural interconversion between agglomerated palladium domains and mononuclear Pd (II) cations in chabazite zeolites, Chem. Mater. 33 (2021) 1698–1713.
[12] Y. Ryou, J. Lee, H. Lee, C.H. Kim, D.H. Kim, Effect of various activation conditions on the low temperature NO adsorption performance of Pd/SSZ-13 passive NOx adsorber, Catal. Today 320 (2019) 175–180.
[13] L. Castoldi, R. Matarrese, S. Morandi, P. Ticali, L. Lietti, Low-temperature Pd/FER NOx adsorbers: operando FT-IR spectroscopy and performance analysis, Catal. Today 360 (2020) 317–325.
[14] K. Khivantsev, N.R. Jaegers, I.Z. Koleva, H.A. Aleksandrov, L. Kovarik, M. H. Engelhard, F. Gao, Y. Wang, G.N. Vayssilov, J. Szanyi, Stabilization of super electrophilic Pd^{+2} cations in small-pore SSZ-13 zeolite, J. Phys. Chem. C (2019) 309–321.
[15] Y. Zheng, L. Kovarik, M.H. Engelhard, Y. Wang, Y. Wang, F. Gao, J. Szanyi, Low-temperature Pd/zeolite passive NOx adsorbers: structure, performance, and adsorption chemistry, J. Phys. Chem. C 121 (2017) 15793–15803.
[16] R. Pace, T.M. Lardinois, Y. Ji, R. Gounder, O. Heintz, M. Crocker, Effects of treatment conditions on Pd speciation in CHA and Beta zeolites for passive NOx adsorption, ACS Omega 6 (2021) 29471–29482.
[17] P. Kim, J. Van der Mynsbrugge, H. Aljama, T.M. Lardinois, R. Gounder, M. Head-Gordon, A.T. Bell, Appl. Catal. B Environ. 304 (2022), 120992.
[18] C. Descorme, P. Gélin, M. Primet, C. Lécuyer, Infrared study of nitrogen monoxide adsorption on palladium ion-exchanged ZSM-5 catalysts, Catal. Lett. 41 (1996) 133–138.
[19] B. Pommier, P. Gelin, Infrared and volumetric study of NO adsorption on Pd-H-ZSM-5, Phys. Chem. Chem. Phys. 3 (2001) 1138–1143.
[20] J. Jacquemin, S. Siffert, J.-F. Lamonier, E. Zhilinskaya, A. Aboukais, Catalytic properties of beta zeolite exchanged with Pd and Fe for toluene total oxidation. Studies in Surface Science and Catalysis, Elsevier, 2002, pp. 699–706.
[21] K. Khivantsev, X. Wei, L. Kovarik, N.R. Jaegers, E.D. Walter, P. Tran, Y. Wang, J. Szanyi, Pd/FER vs Pd/SSZ-13 Passive NOx Adsorbers: Adsorbate-controlled Location of Atomically Dispersed Pd(II) in FER Determines High Activity and Stability, 2020, chemrvix.org, https://chemrxiv.org/engage/chemrxiv/article-details/ 60c74c16469df43dbef43fff.
[22] J. Van der Mynsbrugge, M. Head-Gordon, A.T. Bell, Computational modeling predicts the stability of both Pd^{+} and Pd^{2+} ion-exchanged into H-CHA, J. Mater. Chem. A 9 (2021) 2161–2174.
[23] A. Gupta, S.B. Kang, M.P. Harold, NOx uptake and release on Pd/SSZ-13: impact Of Feed composition and temperature, Catal. Today 360 (2020) 411–425.
[24] M. Ambast, A. Gupta, B.M.M. Rahman, L.C. Grabow, M.P. Harold, NOx adsorption with CO and C2H4 on Pd/SSZ-13: experiments and modeling, Appl. Catal. B Environ. 286 (2021), 119871.

[25] M. Ambast, K. Karinshak, B.M.M. Rahman, L.C. Grabow, M.P. Harold, Passive NOx adsorption on Pd/H-ZSM-5: experiments and modeling, Appl. Catal. B Environ. 269 (2020), 118802.
[26] K. Mandal, Y. Gu, K.S. Westendorff, S. Li, J.A. Pihl, L.C. Grabow, W.S. Epling, C. Paolucci, Condition-dependent Pd speciation and NO adsorption in Pd/zeolites, ACS Catal. (2020) 12801–12818.
[27] K. Khivantsev, N.R. Jaegers, L. Kovarik, J.C. Hanson, F. Tao, Y. Tang, X. Zhang, I. Z. Koleva, H.A. Aleksandrov, G.N. Vayssilov, Achieving atomic dispersion of highly loaded transition metals in small-pore zeolite SSZ-13: high-capacity and high-efficiency low-temperature CO and passive NOx adsorbers, Angew. Chem. 130 (2018) 16914–16919.
[28] Y. Ryou, J. Lee, Y. Kim, S. Hwang, H. Lee, C.H. Kim, D.H. Kim, Effect of reduction treatments (H2 vs. CO) on the NO adsorption ability and the physicochemical properties of Pd/SSZ-13 passive NOx adsorber for cold start application, Appl. Catal. A Gen. 569 (2019) 28–34.
[29] Y. Gu, R.P. Zelinsky, Y. Chen, W.S. Epling, Investigation of an irreversible NOx storage degradation mode on a Pd/BEA passive NOx adsorber, Appl. Catal. B Environ. 258 (2019), 118032.
[30] J. Theis, J. Ura, Assessment of zeolite-based low temperature NOx adsorbers: Effect of reductants during multiple sequential cold starts, Catal. Today 360 (2021) 340–349.
[31] J.R. Di Iorio, R. Gounder, Controlling the isolation and pairing of aluminum in chabazite zeolites using mixtures of organic and inorganic structure-directing agents, Chem. Mater. 28 (2016) 2236–2247.
[32] J.R. Di Iorio, C.T. Nimlos, R. Gounder, Introducing catalytic diversity into single-site chabazite zeolites of fixed composition via synthetic control of active site proximity, ACS Catal. 7 (10) (2017) 6663–6674.
[33] J.R. Di Iorio, S. Li, C.B. Jones, C.T. Nimlos, Y. Wang, E. Kunkes, V. Vattipalli, S. Prasad, A. Moini, W.F. Schneider, R. Gounder, Cooperative and competitive occlusion of organic and inorganic structure-directing agents within chabazite zeolites, J. Am. Chem. Soc. 142 (2020) 4807–4819.
[34] V.Y. Prikhodko, J.A. Pihl, T.J. Toops, J.E. Parks, Passive SCR performance under pseudo-transient cycle: challenges and opportunities for meeting tier 3 emissions, Emiss. Control Sci. Technol. 5 (2019) 253–262.
[35] P. Chambon, S. Huff, K. Norman, K.D.D. Edwards, J. Thomas, V.Y. Prikhodko, European Lean Gasoline Direct Injection Vehicle Benchmark SAE Tech. Pap., 2011, 2011, 01, 1218.
[36] J.E. Parks, V. Prikhodko, W. Partridge, J.-S. Choi, K. Norman, S. Huff, P. Chambon, Lean gasoline engine reductant chemistry during lean NOx trap regeneration, SAE Int. J. Fuels Lubr. 3 (2010) 956–962.
[37] K.G. Rappé, C. DiMaggio, J.A. Pihl, J.R. Theis, S.H. Oh, G.B. Fisher, J. Parks, V. G. Easterling, M. Yang, M.L. Stewart, K.C. Howden, Aftertreatment protocols for catalyst characterization and performance evaluation: low-temperature oxidation, storage, three-way, and NH3-SCR catalyst test protocols, Emiss. Control Sci. Technol. 5 (2019) 183–214.
[38] M. Ambast, A. Gupta, B.M.M. Rahman, L.C. Grabow, M.P. Harold, "NOx adsorption with CO and C_2H_4 on Pd/SSZ-13: experiments and modeling", Appl. Catal. B: Environ. 286 (2021), 119871.
[39] A. Gupta, S.B. Kang, M.P. Harold, NOx uptake and release on Pd/SSZ-13: impact of feed composition and temperature, Catal. Today 360 (2021) 411–425.
[40] K. Khivantsev, N. Jaegers, L. Kovarik, S. Prodinger, M. Derewinski, Y. Wang, F. Gao, J. Szanyi, Palladium/Beta zeolite passive NOx adsorbers (PNA): clarification of PNA chemistry and the effects of CO and zeolite crystallite size on PNA performance, Appl. Catal. A: Gen. 569 (2019) 141–148.
[41] Y. Gu, S. Sinha Majumdar, J.A. Pihl, W.S. Epling, Investigation of NO adsorption and desorption phenomena on a Pd/ZSM-5 passive NOx adsorber, Appl. Catal. B: Environ. 298 (2021), 120561.